TB, BPN, PMB/235205, 14/02/2007

IOP PUBLISHING PHYSICS IN MEDICINE AND BIOLOGY

Phys. Med. Biol. **52** (2007) 1–14 UNCORRECTED PROOF

Eye rotation induced dynamics of a Newtonian fluid within the vitreous cavity: the effect of the chamber shape

Alessandro Stocchino[1], Rodolfo Repetto[2,3] and Chiara Cafferata[1]

[1] Department of Environmental Engineering, University of Genoa, Italy
[2] Department of Engineering of Structures, Water and Soil, University of L'Aquila, Italy

E-mail: jorma@diam.unige.it

Received 17 October 2006, in final form 8 January 2007
Published DD MMM 2007
Online at stacks.iop.org/PMB/52/1

Abstract

The dynamics of the vitreous body induced by eye rotations is studied experimentally. In particular, we consider the case in which the vitreous cavity is filled by a Newtonian fluid, either because the vitreous is liquefied or because it has been replaced, after vitrectomy, by a viscous fluid. We employ a rigid Perspex container which models, in a magnified scale, the vitreous cavity of the human eye. The shape of the cavity closely resembles that of the real vitreous chamber; in particular, the anterior part of the container is concave in order to model the presence of the eye lens. The container is filled with glycerol and is mounted on the shaft of a computer-controlled motor which rotates according to a periodic time law. PIV (particle image velocimetry) measurements are taken on the equatorial plane orthogonal to the axis of rotation. The experimental measurements show that the velocity field is strongly influenced by the deformed geometry of the domain. In particular, the formation of a vortex in the vicinity of the lens, which migrates in time towards the core of the domain, is invariably observed. The vortex path is tracked in time by means of a vortex identification technique and it is found that it is significantly influenced by the Womersley number of the flow. Particle trajectories are computed from the PIV measurements. Particles initially located at different positions on the equatorial horizontal plane (perpendicular to the axis of rotation) tend to concentrate in narrow regions adjacent to the lens, thus suggesting the existence, in such regions, of a vertical fluid ejection. Such a strong flow three-dimensionality, which is essentially induced by the irregular shape of the domain, may play a significant role in the mixing processes taking place inside the eye globe. The tangential stresses acting on the rigid boundary of the domain are also computed from the experimental measurements showing that regions subject to particularly intense stresses exist along the boundary close to the lens.

[3] On sabbatical at the Department of Bioengineering, Imperial College London, UK.

1. Introduction

The vitreous body is the largest structure of the eye, making up approximately 80% of its total volume. It fills the vitreous cavity and is delimited anteriorly by the lens and posteriorly by the retina. The mature vitreous is a transparent gel with viscoelastic rheological properties (Lee *et al* 1992). The vitreous typically goes through significant mechanical changes during life: the normal vitreous in youth is a homogeneous gel and the fundamental ageing process consists of a progressive disintegration of the gel structure, more so at the centre of the vitreous cavity. Such a process is referred to as vitreous liquefaction and it may be so extensive as to involve the whole vitreous cavity.

The vitreous, along with other physiological roles, has the following main mechanical functions: (i) securing the retina's adherence to the outer layers and filling-up the vitreous chamber; (ii) acting as a barrier between the anterior and the posterior segments of the eye for heat and drug transport (Lund-Andersen 2003). It is reasonable to expect that the relative motion of the vitreous with respect to the vitreous cavity wall, induced by rapid eye rotations, may affect the efficiency of the vitreous body in performing both the above functions. Under normal circumstances the vitreous is a gel which undergoes little flow with respect to the vitreous chamber. On the other hand, if the vitreous is partially or completely liquefied or if it is replaced, after vitrectomy, by other fluids, such as saline or silicone oil, its motion may be quite intense. Therefore, from the fluid dynamics point of view, these conditions are particularly worth attention (Canning *et al* 2002).

Let us briefly discuss how the dynamics of the vitreous body may affect its capability to fulfil the mechanical functions mentioned above. We first consider the vitreous role of supporting the retina. Many authors have postulated a possible connection between the occurrence of a retinal detachment (RD) and the fluid dynamic events within the vitreous chamber. In particular, the shear stress exerted by the vitreous (or by tamponade fluids in vitrectomized eyes) on the retina is thought to be an important factor in inducing RD. This has motivated some research on the dynamics of the vitreous motion induced by eye rotations. The most significant contributions in this field are cited in Repetto (2006) to which the reader is referred. Here we will just recall the works by David *et al* (1998) and Repetto *et al* (2005). David *et al* (1998) proposed an analytical model of vitreous dynamics. Their work is based on the assumption of small-amplitude sinusoidal eye rotations. The vitreous cavity is assumed to be spherical and the vitreous rheology is modelled according to Lee *et al*'s (1992) results. David *et al* (1998) found that the shear stress at the wall increases linearly with the sphere radius and they argued that this may explain the more frequent occurrence of RD in myopic eyes, which are typically of a larger size. Repetto *et al* (2005) studied experimentally the motion of a Newtonian fluid within a rotating sphere. They performed experiments both rotating the sphere according to a periodic time law and reproducing real single saccadic movements. Their results confirm the validity of David *et al*'s (1998) approach. The authors also find that the maximum shear stress at the wall is almost independent of the amplitude of the saccadic movement and it strongly increases with increasing values of the fluid viscosity.

In both the above studies the vitreous cavity is described as a sphere. As a matter of fact, however, the vitreous chamber is not spherical but rather concave in the anterior part, due to the presence of the lens. Even a weak departure from the spherical shape may induce major changes in the flow field and, in turn, may significantly affect the shear stress distribution at the wall. The only attempt to account for this effect is due to Repetto (2006). His analysis is carried out analytically in the limit of low viscosity fluid and the vitreous cavity is described as a weakly deformed sphere. The author's results show that the irregular shape of the domain produces a complex and strongly three-dimensional flow field. The stress distribution at the

wall, which is not computed in the author's model since the flow within the boundary layer at the wall is not accounted for, is also expected to be strongly affected by the shape of the vitreous chamber.

Let us now discuss how the vitreous motion may affect its efficiency to act as a heat and drug barrier between the anterior and the posterior segments of the eye. Quite a few papers in the medical literature have faced the problem of analysing the transport phenomena within the vitreous cavity; the reader is referred to Lund-Andersen (2003) for a thorough review. As far as the transport of solutes is concerned *in vivo* measurements are possible by using fluorescein as a tracer and performing vitreous fluorophotometry. Such measurements are invariably interpreted in terms of a diffusion process, with the aim of determining an overall diffusion coefficient. The diffusive process of heat transfer within the vitreous body has been studied numerically by many authors (e.g., Scott (1988), Cicekli (2003) and Flyckt *et al* (2006)). All the existing works consider the transport processes within the vitreous as being purely diffusive; however, the motion of the vitreous induced by eye rotation is also responsible for a convective transport and, if vitreous mixing is intense enough, advection may be by far a more efficient process. This idea is supported by the clinical observation that, in normal conditions, the vitreous is much more efficient as a transport barrier than in the case of liquefied vitreous or in vitrectomized eyes and, in both the aforementioned circumstances, the fluid dynamic processes in the vitreous cavity are much more intense even though, admittedly, the diffusive coefficient of the healthy vitreous may also be different from that of the liquefied vitreous or of tamponade fluids. In order to evaluate the advection processes within the vitreous cavity a full understanding of the flow field characteristics is firstly required. In this respect, the work by Repetto (2006) suggests that the non-sphericity of the vitreous chamber plays an essential role in generating a three-dimensional flow field and, consequently, in inducing intense fluid mixing.

In the present work we extend the work by Repetto *et al* (2005) and present experimental results of the vitreous motion within a cavity which closely resembles the real vitreous cavity shape. A Newtonian fluid is employed, thus the elastic properties of the vitreous are disregarded at this stage. However, the experimental conditions reproduce both the case of liquefied vitreous and the case of post vitrectomy eyes, which, as discussed above, are those in which the hydrodynamic events within the vitreous cavity are most intense.

2. Experimental setup and procedures

The apparatus used for the present experiments is identical to the one employed in Repetto *et al* (2005) to which the reader is referred for a detailed description (see figure 2 of Repetto *et al*'s paper for a sketch of the experimental apparatus). The eye model is mounted on the shaft of an electrical motor that is controlled by external signals, suitably built in order to reproduce a prescribed time-dependent motion.

In the present work we focus our attention on sinusoidal rotations of the eye model around a vertical axis, with period T, frequency f and amplitude a, under the assumption that a sequence of saccadic movements with alternate directions may be modelled, in a highly simplified manner, as a sinusoidal motion, the duration of each saccade being equal to half of the rotation period. Even though such an approach has been adopted by most previous authors, we are aware that this is a fairly idealized way of modelling real saccadic movements (see Repetto *et al* (2005) for a discussion on saccadic eye rotations). Nevertheless, in order to understand the basic features of the flow field it is better to restrict the experimental conditions to such simple movements; the present results will help to understand the flow features induced by more complex and realistic rotations of the container. The dimensionless parameters which

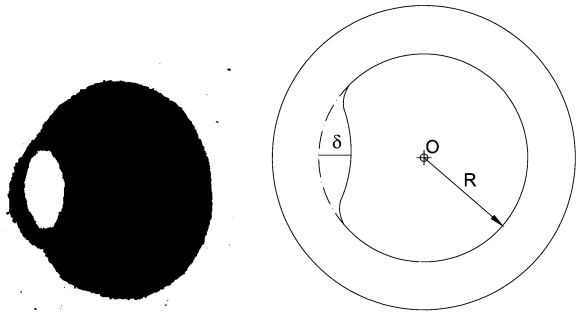

Figure 1. Left: a false-coloured magnetic resonance image of the equatorial plane of a human eye. Right: cross section along the equatorial plane of the Perspex physical model used in the present experiments. The container is rotated about the vertical axis (orthogonal to the plane of the drawing) passing through point O.

govern the problem are the amplitude of rotations a and the Womersley number (Loudon and Tordesillas 1998), defined as

$$\alpha = \sqrt{\frac{R^2\omega}{\nu}}, \tag{1}$$

where R is a characteristic radius of the container, ν is the kinematic viscosity of the fluid and $\omega = 2\pi/T = 2\pi f$ is the angular frequency. The Womersley number characterizes the unsteady fluid flow response to a time periodic forcing and can be physically interpreted as the ratio between the characteristic dimension of the domain (R in the present case) and the thickness of the Stokes-type boundary layer at the wall, whose order of magnitude is $\sqrt{\nu/\omega}$.

For the present purpose of investigating the role of the shape of the eye globe, a set of Perspex models have been specifically designed. Several images of normal human eyes, taken from ultrasound and magnetic resonance scans, were analysed, showing that the departure of the vitreous cavity from the spherical shape is essentially due to two recurring features: first, the antero-posterior axis is slightly shorter than the other two and secondly the lens produces an indentation such that, in the anterior segment, the domain concavity faces inward. The latter effect is by far more significant and, in order to isolate its role on the flow characteristics, it is the only one accounted for in the present study. The shape of the eye is thus reproduced as a sphere of radius R (equal to 40.8 mm in our model) with a deformation on one side representing the lens, modelled as a spherical cap with its apex pointing towards the centre of the globe. The two spheres are smoothly connected. In figure 1 a magnetic resonance image of the horizontal equatorial plane of a human eye is reported, together with a drawing of the same plane of the Perspex model employed, showing that the model resembles the real shape of the human vitreous chamber with a fairly good approximation. The size of the spherical cap δ, i.e. the maximum radial departure of the actual geometry from the spherical shape, has been varied so as to obtain the values 0.15, 0.2 and 0.3 for the ratio δ/R (see figure 1). Most of the experiments were conducted employing the 'large lens' container ($\delta/R = 0.3$) since it is the one which most closely resembles the real shape of the vitreous cavity.

We have performed three series of experiments. In the first set, denoted as s1, we have reproduced sinusoidal rotations with the same amplitude and variable frequency, spanning in this way a range of Womersley number values from about 4.5 up to 15. This range is representative of real eye movements if the viscosity of normal ($\nu \approx 1.410^{-4}$ m^2 s^{-1}) or liquefied vitreous ($\nu \approx 10^{-6}$ m^2 s^{-1}) is considered; the fluid motion in eyes in which the

Table 1. Main parameters of the experiments performed.

Experiment number	a (°)	α	f (Hz)	ν (10^{-4} m^2 s^{-1})	δ/R
1-s1	20	4.32	1	5.59	0.3
2-s1	20	5.97	2	5.87	0.3
3-s1	20	7.60	3	5.43	0.3
4-s1	20	8.74	4	5.48	0.3
5-s1	20	9.79	5	5.45	0.3
6-s1	20	10.87	6	5.31	0.3
7-s1	20	11.74	7	4.98	0.3
8-s1	20	12.96	8	4.50	0.3
9-s1	20	14.49	9	4.48	0.3
10-s1	20	12.39	10	6.81	0.3
11-s1	20	15.03	11	5.01	0.3
1-s2	10	3.63	1	7.91	0.3
2-s2	10	7.27	4	7.91	0.3
3-s2	10	9.62	7	7.91	0.3
4-s2	20	3.71	1	7.60	0.3
5-s2	20	7.37	4	7.60	0.3
6-s2	20	9.82	7	7.60	0.3
7-s2	30	3.69	1	7.70	0.3
8-s2	30	7.37	4	7.70	0.3
9-s2	30	9.82	7	7.70	0.3
10-s2	40	3.71	1	7.70	0.3
11-s2	40	7.37	4	7.70	0.3
12-s2	40	9.82	7	7.70	0.3
1-s3	20	8.48	4	5.40	0.2
2-s3	20	8.48	4	5.40	0.15

vitreous has been replaced by tamponade fluids also falls close this range (for silicone oils $\nu \approx 10^{-3}$ m^2 s^{-1}). Indeed, for a sequence of saccades with the characteristics described in Becker (1989), the angular frequency ω assumes values from $\approx$20 s^{-1} for large eye rotations up to $\approx$60 s^{-1} or more for small amplitude rotations. In the case of liquefied vitreous or post-vitrectomy eyes, when the vitreous cavity is eventually filled with aqueous humour, much higher values of the Womersley number may be reached. The limitations of the experimental apparatus, however, precluded the possibility of investigating these conditions. A second set of experiments, denoted as s2, had the purpose to study the role of the amplitude of rotations for a fixed Womersley number; finally, a few further experiments (series s3) were aimed at investigating the effect of different lens sizes. In table 1 the dimensional and dimensionless parameters for each of the performed experiments are reported.

As in our previous work (Repetto *et al* 2005), the rotation of the eye physical model is synchronized with a two-dimensional particle image velocimetry (PIV) acquisition system, used to measure two-dimensional velocity fields on the equatorial plane orthogonal to the axis of rotation. We focus our attention on such a plane since, for symmetry reasons, the velocity vectors are there expected to lie on the measurement plane, which is the ideal condition for the PIV technique. The same optical arrangement as in Repetto *et al* (2005) has been employed to illuminate the equatorial plane of the model. It is worth mentioning how image masking, a necessary step in PIV analysis anytime measurements are performed over domains smaller than the entire image plane, has been treated in this case where the shape of the boundary is not regular and varies in time. Each pair of images has been preprocessed before performing the

cross-correlation analysis, applying an edge detection algorithm able to recognize the actual boundary of the measurement domain. In particular, a technique based on the search of the zero-crossings of the image intensity Laplacian has been implemented with very good results.

The sampling rate chosen in the present experiments was such to produce 100 vector fields within a period for the lowest frequency experiments and 50 for the highest frequency runs. The resulting averaged velocity fields $[U(x, y, t), V(x, y, t)]$, where $U(x, y, t)$ and $V(x, y, t)$ are the averaged velocity components in the x and y directions respectively, have been obtained performing an ensemble average over fifty instantaneous velocity fields, with resulting values of the root mean square velocities u_{RMS} and v_{RMS} of the order of a few per cent. The spatial resolution of the measurements obtained based on the PIV settings employed was of one vector per 1.5 mm^2.

In the remaining part of this section we define some quantities computed from the two-dimensional velocity fields that will be employed in the following.

Firstly, we have analysed the flow fields with the aim of detecting possible vortical structures generated during the eye model rotation. Among the different techniques of vortex identification available in the literature, the algorithm presented in Graftieaux *et al* (2001) has proved to be particularly efficient in the present case. Vortices are identified by plotting contour lines of the function Γ which is defined, at a generic point P, as

$$\Gamma(P) = \int\!\!\int_S \sin\theta_M \, \mathrm{d}S, \tag{2}$$

where S is an area surrounding P, the generic point M lies in S, θ_M represents the angle between the velocity vector in M and the radius vector $\overrightarrow{PM}$. Γ is a scalar function such that $|\Gamma| \leqslant 1$ and values of $|\Gamma|$ close to its bound correspond to the vortex centre, the sign of the function being obviously related to the rotation sign of the vortex. We have assumed the area S to have a square shape which contains 20 measured velocity vectors and is centred at the point P. Note that, as stated by Graftieaux *et al* (2001), the number of points contained in the area S has a weak influence on the location of the maxima of the function Γ.

Secondly, we have computed the distribution of the tangential stress τ at the wall on the equatorial plane. We have only considered the deviatoric part of the stress tensor $\mathbf{T}_d$, namely $\mathbf{T}_d = 2\mu\mathbf{D}$ for a Newtonian fluid, with μ being the dynamic viscosity of the fluid and $\mathbf{D}$ the rate of strain tensor defined as the symmetric part of the velocity gradient tensor $\nabla\mathbf{u}$. The evaluation of $\mathbf{T}_d$ requires the determination of first spatial derivatives of the measured velocity field. It is well known that this is a quite delicate operation since derivation enhances measurement noise. Derivatives of the generic velocity component are computed through the second-order least-squares scheme. Starting from the discretized boundary $\mathfrak{F}$ of the equatorial plane, obtained with the edge detection algorithm described above, we have computed numerically the normal inward unit vector $\mathbf{n} = -\nabla\mathfrak{F}/|\nabla\mathfrak{F}|$ and the tangential unit vector $\mathbf{t} = (n_y, -n_x)$ (positive when rotating in the counter clockwise direction with respect to the centre). The tangential stress τ is then obtained as $(\mathbf{n} \cdot \mathbf{T}_d) \cdot \mathbf{t}$.

3. Description of the flow field

Let us now investigate the flow field which is generated within the container subject to periodic rotations. In figures 2(a)–(d) and 3(a)–(d) velocity vector fields are shown at different times for the runs exp-1-s1 ($\alpha = 4.32$, $a = 20^\circ$) and exp-7-s1 ($\alpha = 11.74$, $a = 20^\circ$). At a first glance it appears that the indentation at the anterior part of the vitreous cavity model significantly affects the flow field. In particular, approximately at times $t \approx 0$, i.e. when the container reaches the maximum angular velocity, a vortex structure is present close to the lens. In all the plots

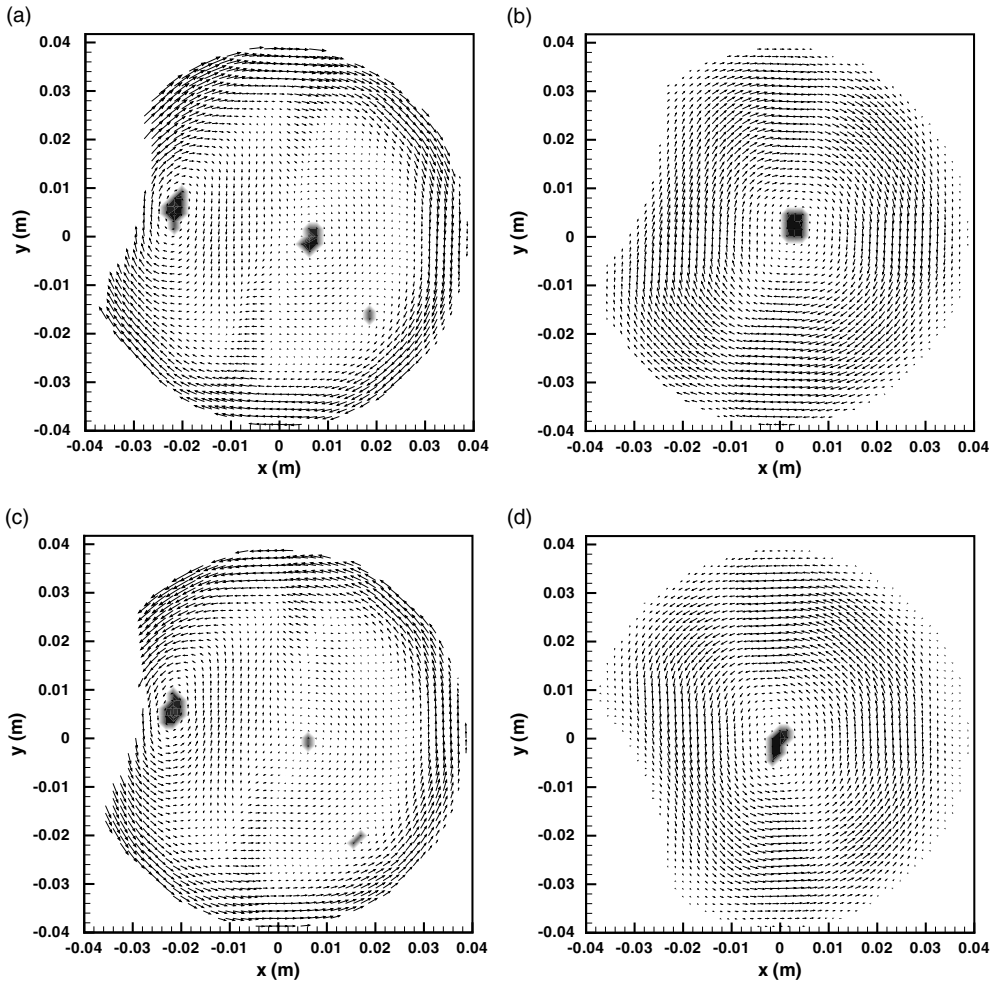

Figure 2. Flow fields on the equatorial plane at four different times (exp-1-s1, $\alpha = 4.32$, $a = 20^{\circ}$). Contour lines refer to the scalar function Γ defined by equation (2). (a) $t \approx 0$ (maximum container angular velocity), (b) $t \approx 1/4T$, (c) $t \approx 1/2T$, (d) $t \approx 3/4T$.

reported in figures 2(a)–(d) and 3(a)–(d) the existence and position of the vortex is enlightened by plotting contour lines of the function Γ defined by equation 2. From the observation of the sequence of plots reported in the figures it appears that the vortex is generated close to the lens and then it progressively migrates towards the core of the domain, where it is eventually dissipated. A new vortex is then generated close to the lens with an opposite sign of rotation during the second half of the period. The generation of such a vortical structure is invariably observed during all the experiments performed, regardless of the amplitude of the sinusoidal motion, of the Womersley number and of the size of the lens.

The path followed by the vortex, relative to the container, however, is strongly dependent on α. At low values of such a parameter (figures 2(a)–(d)) the flow is symmetrical with respect to the container indentation, no wake effect is observed in the rear part of the moving lens and, in this case, the vortex migrates roughly along a straight pattern from the apex of the lens

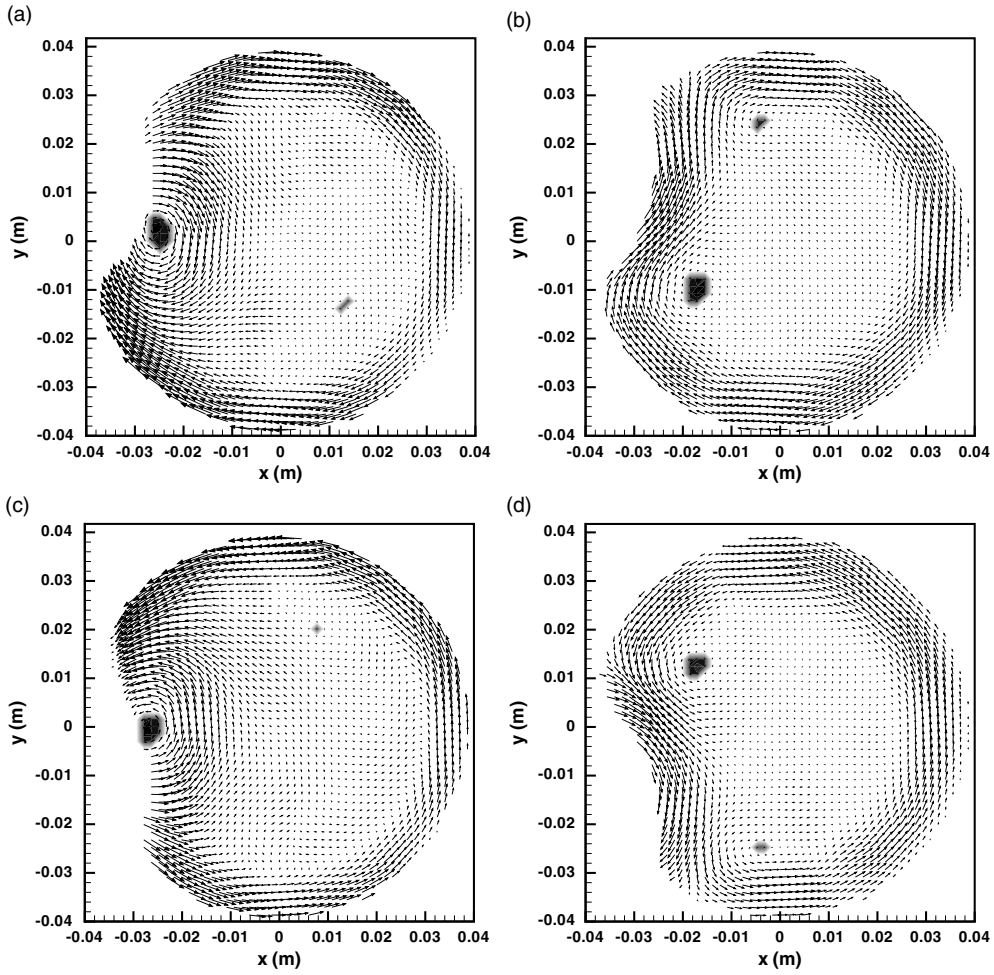

Figure 3. Flow fields on the equatorial plane at four different times (exp-7-s1, $\alpha = 11.74$, $a = 20^{\circ}$). Contour lines refer to the scalar function Γ defined by equation (2). (a) $t \approx 0$ (maximum container angular velocity), (b) $t \approx 1/4T$, (c) $t \approx 1/2T$, (d) $t \approx 3/4T$.

towards the centre of the globe. As the Womersley number of the flow increases, differences between the flow in the regions upstream and downstream of the lens become visible (see figures 3(a)–(d)) and such an asymmetry of flow conditions is responsible for a deviation of the vortex path. In this case the vortex does not move towards the centre nor the trajectory it follows is straight. Consequently, at each cycle, the dissipation of the vortex does not occur at the centre of the domain anymore.

The differences between vortex trajectories at low and high values of the Womersley number are clearly shown in figure 4 (left). In the figure the path relative to the container covered by the vortex, identified by the position of the vortex core, is shown for different experiments varying α and keeping a constant. It appears that the greater the value of α the stronger the deviation of the vortex trajectory from the straight line connecting the apex of the lens to the centre of the container. Moreover, figure 4 (right) shows that for given values of

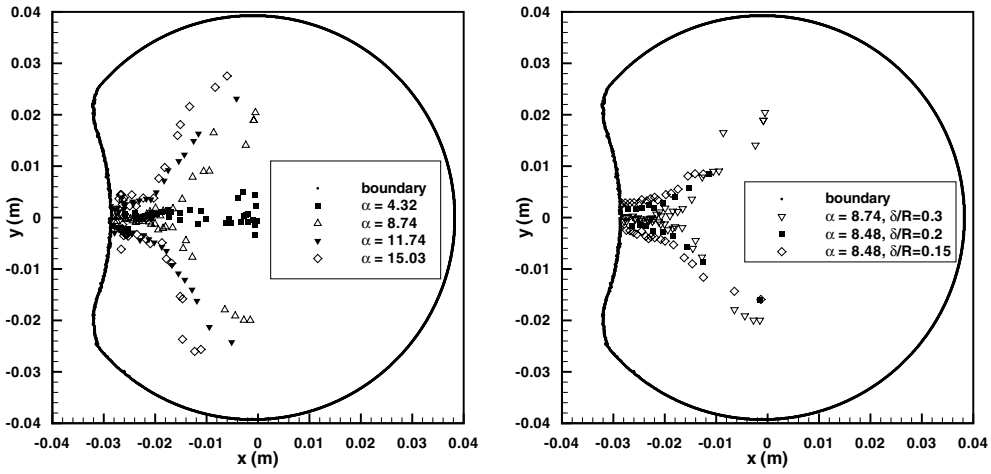

Figure 4. Trajectories relative to the container wall covered by the vortex centre during a cycle. Left: different values of the Womersley number α ($a = 20^\circ$, $\delta/R = 0.3$). Right: different values of δ/R ($a = 20^\circ$, $f = 4$ Hz, $\alpha \approx 8.5$).

α and a, the size of the indentation does not strongly influence the evolution of the vortical structures.

The vortex structure described above originates at time $t \approx 0$ (corresponding to the maximum container angular velocity) when there is a region, fairly close to the lens, where velocity vectors are directed in the opposite sense with respect to the wall motion and, consequently, also with respect to the velocity of the fluid located in the immediate vicinity of the wall. A similar flow pattern close to the lens can be inferred from the theoretical predictions of Repetto (2006), obtained in the limit of low values of the fluid viscosity. The irrotational flow within the weakly deformed rotating sphere considered by the author is such that, close to the lens, the velocity is in the opposite direction with respect to the motion of the wall. If the flow within the boundary layer adjacent to the wall is accounted for this situation leads to the generation of a vortex structure similar to that observed in our experiments.

More insight into the characteristics of the flow field generated within the rotating eye model can be obtained by computing particle trajectories from the PIV measurements. This is done by integrating in time the measured velocity fields. The time integration is performed adopting an explicit fourth-order Runge–Kutta scheme and spatial velocity vectors are interpolated using a cubic polynomial interpolation algorithm. The above numerical integration is a delicate operation and might be affected by errors due to the following reasons: first, we integrate an experimental velocity field that is by definition affected by some error; second, the integration time step is set by the PIV acquisition rate. Having in mind these possible sources of uncertainty, the computed trajectories still represent, with a good approximation, the paths followed by a fluid particle inside the domain. A better evaluation of particle trajectories can be achieved by direct measurement through the particle tracking velocimetry technique; this is actually planned as a future activity.

In figure 5(a) particle paths relative to the container, sampled with a time step equal to the cycle period T, are plotted starting from different initial locations within the domain (exp-5-s1, $\alpha = 9.79, a = 20^\circ$). A quite interesting pattern appears. Starting from different positions on the equatorial plane particles tend to move towards a region located close to the anterior

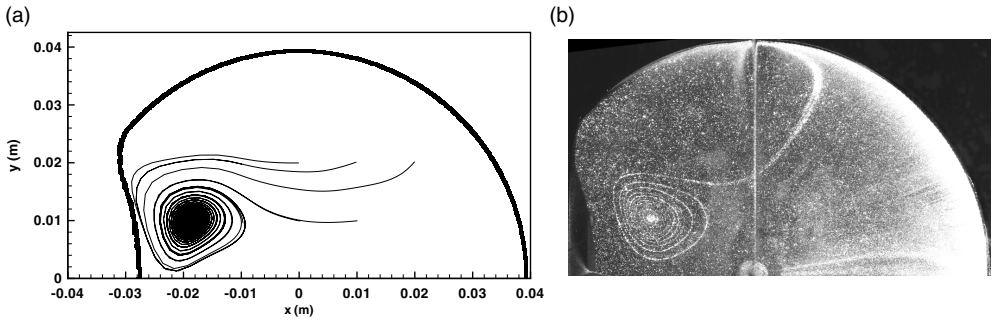

Figure 5. (a) relative particle paths sampled every cycle; (b) flow field structure visualization obtained by injecting a higher particle concentration at a certain position (exp-5-s1, $\alpha = 9.79$, $a = 20^{\circ}$).

segment of the eye model. Clearly, for the continuity principle to be satisfied, an ejection of fluid in such a region must occur in the direction orthogonal to the measurement plane. Note that quite a few rotation periods (of the order of a hundred cycles on the average) are required for a full trajectory to be completed by a particle. The existence of a region of particle concentration is nicely shown in figure 5(b), which is an instantaneous picture shot after having rotated the container for some tens of cycles. The light curves which can be observed are due to an initially higher concentration of particle tracers in a certain region of the domain. Note that these curves represent streaklines rather than particle trajectories. However, since we are dealing with a periodic motion and the trajectories are built sampling every of period of rotation, streaklines and trajectories coincide in this case (see, for instance, Ottino (1989)).

In figures 6 particle paths relative to different values of the Womersley number are reported. For all values of α, particles tend to concentrate in the anterior part of the eye globe, regardless of their initial position. However, at low values of the Womersley number, i.e. when the flow field is remarkably symmetrical with respect to the axis $y = 0$, particles tend to concentrate close to the apex of the lens. On the other hand, as the value of the Womersley number increases, the generation of two distinct cells clearly appears, probably generated by the incipient flow asymmetry. The cells pattern is symmetrical with respect to the axis $y = 0$, and the cells seem to (slightly) move apart as α increases. This is possibly related to the different paths followed by the vortical structures during the container rotation, as discussed above.

The above observations show that the flow field generated by the container rotations has a very complex three-dimensional structure. A three-dimensional flow field was also observed in the case of a perfectly spherical rotating container considered by David *et al* (1998) and Repetto *et al* (2005). Indeed, the above authors describe the formation of two slowly rotating toroidal vortices whose formation is essentially induced by the spherical shape of the container. However, the vertical velocity components associated with such three-dimensional structures are found to be various orders of magnitude ($\sim$4) smaller than the velocity components on planes perpendicular to the axis of rotation. David *et al* (1998) point out the importance of such a secondary motion in inducing a complete mixing of the fluid over large time scales. In the present case, similar structures also form and have indeed been observed by flow visualizations similar to those described by Repetto *et al* (2005). However, the vertical fluid ejections described above, which are entirely related to the presence of the indentation in the anterior part of the cavity, generate a much more intense overall mixing of the fluid and

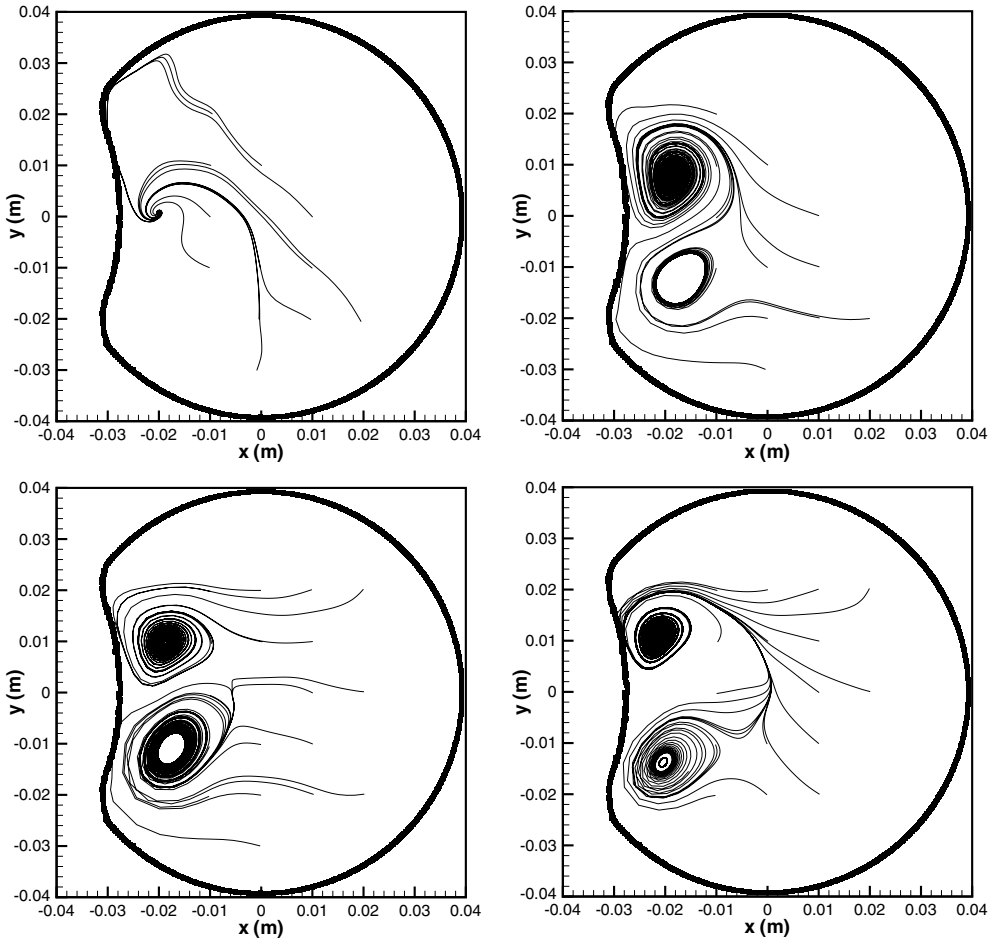

Figure 6. Relative particle paths sampled every cycle for different values of the Womersley number and constant amplitude $a = 20^\circ$. From top left to bottom right, $\alpha = 4.32$, 7.60, 9.79 and 11.74.

are likely to be responsible of strong advection processes within the vitreous cavity. This confirms the speculations anticipated in the introduction that advective transport within the vitreous cavity is probably much more efficient than pure diffusion when the vitreous dynamics is intense enough, i.e. when the vitreous has lost its elastic properties (as a consequence of vitreous liquefaction or vitreous substitution with purely viscous tamponade fluids).

4. Shear stress at the wall

As described in the introduction, it is believed that the shear stress exerted by the vitreous on the retina may play an important role in the RD mechanism. In this respect it is important to understand what the influence of the vitreous cavity shape on the stress distribution at the wall is. In particular, it is important to ascertain whether regions of the boundary exist which are subject to high stresses. In the present section we discuss the stress distribution within the equatorial plane orthogonal to the axis of rotation.

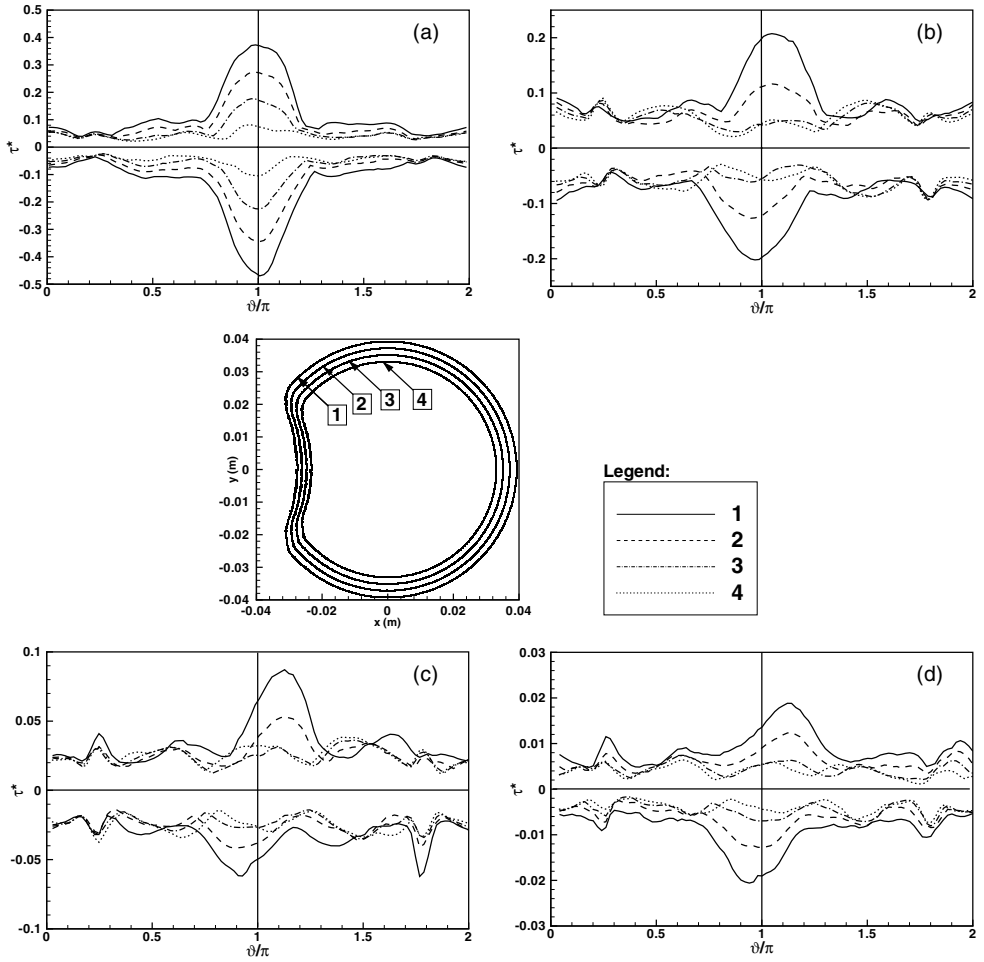

Figure 7. Distribution of the maximum dimensionless tangential stress $\tau^* = \tau/(\rho\omega^2 R^2)$ as a function of the angle ϑ/π along the four different concentric boundaries shown in the central panel ($a = 20^\circ$). (a) $\alpha = 4.32$, (b) $\alpha = 8.74$, (c) $\alpha = 11.74$, (d) $\alpha = 15.03$. The correspondence between shear stress profiles and the boundary is indicated in the central legend.

In order to obtain a picture of the stress distribution on the equatorial plane of the domain, we plot the shear stress τ exerted by the fluid along the concentric curves depicted in figure 7, labelled 1, 2, 3 and 4 moving towards the centre of the eye model. These curves are obtained by progressively contracting the wall profile to the axis of rotation. All such curves are spanned by the angular coordinate ϑ, the origin of which is assumed such that $\vartheta = \pi$ at the apex of the lens.

In figures 7(a)–(d) we report the maximum and minimum tangential stresses reached during a cycle along such curves. Note that, from the clinical point of view, the most interesting quantities to be evaluated are the extremal values of the shear stress on the retina, i.e. on the cavity walls. The labels in the legend of figures 7(a)–(d) allow us to associate each shear stress distribution with the curve on which the stress is computed. In all plots the shear stress is made dimensionless with $\rho\omega^2 R^2$. Each plot is relative to a different value of the

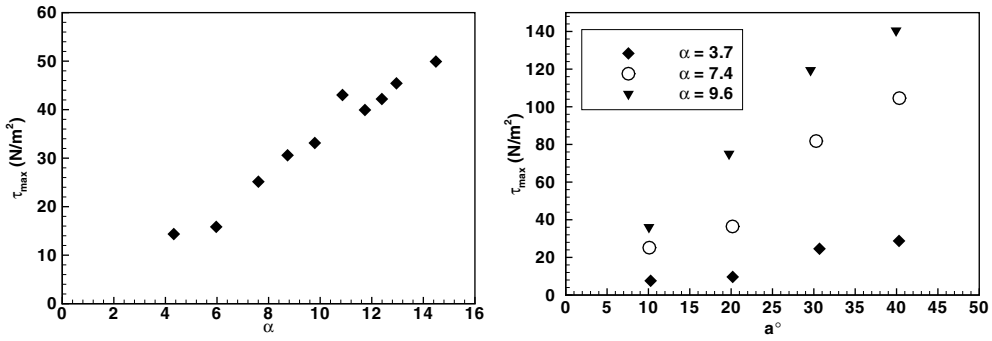

Figure 8. Maximum value of the dimensional tangential stress τ_{max} on the boundary of the eye globe model as a function of the Womersley number α (left panel, $a = 20^\circ$) and of the amplitude of rotations a (right).

Womersley number and the amplitude of the rotations a is constant. It clearly appears that the presence of the lens has a great influence on the shear stress distribution at the wall, especially at low values of the Womersley number. In particular, a clear stress peak is invariably observed close to the lens, where the maximum shear stress may well be up to five times larger than in most of the container wall. On the other hand, within the range $0.7 < \vartheta/\pi < 1.3$ the extreme values of the shear stress at the wall reached during each cycle remain fairly constant. As we move towards the centre of the eye model the influence of the lens weakens and the shear stress distribution tends to become constant.

It is interesting to note that the shear stress at the wall peaks at different locations for different values of the Womersley number of the flow. In particular, at low α, the maximum tangential stress is located almost exactly at the lens ($\vartheta = \pi$), as shown in figure 7(a). As α increases (figures 7(b)–(d)) the location of the maximum shear stress progressively moves away from the lens in the upstream direction. This is a further effect of the asymmetry of the flow field with respect to the lens which is observed at high values of the Womersley number.

Finally, in figures 8 the maximum dimensional shear stress at the wall τ_{max}, reached during the entire rotation period is shown as a function of the Womersley number (left) and of the amplitude of the container rotations (right). As one might expect it appears that τ_{max} increases, almost linearly, with both α and a.

5. Conclusions and future developments

In the present paper we investigated the motion induced in the vitreous body by eye rotations, focusing in particular on the effect of the vitreous cavity shape on flow characteristics.

Results suggest that the irregular shape of the vitreous chamber, due to the presence of the lens in the anterior segment of the eye, is responsible for the generation of a complex three-dimensional flow field. In particular, in all experiments, the generation and migration of a vortex structure within the eye has been observed. The vortex path has been tracked in time, showing its strong dependence on the Womersley number of the flow. Whether such a vortex has any significance from the clinical point of view is a challenging question for the applied clinical researcher. Certainly, though, it has a strong influence both on the shear stress distribution on the vitreous chamber wall and, in particular, on the mixing processes taking place within the vitreous.

Particle trajectories computed from the measured flow fields show that particles on the equatorial plane orthogonal to the axis of rotation tend to concentrate within narrow regions located close to the lens. In these regions the fluid is therefore vertically ejected and this produces a highly three-dimensional circulation within the vitreous cavity. This clearly indicates the existence of an efficient mixing process. This observation suggests that advection should be accounted for in order to study transport phenomena within the vitreous cavity. As a matter of fact, advection induced by such a complex flow field will invariably produce a highly non-isotropic transport, which can hardly be described by means of a single diffusion coefficient as done in all existing studies on the subject.

The present work provides a detailed description of the flow field within the vitreous cavity on the equatorial plane and demonstrates the existence of interesting hydrodynamic phenomena which will deserve future attention. Three-dimensional measurements (not very easy to conduct) and numerical simulations will be needed in future to complete the picture.

Finally, from the measured flow fields the viscous stresses at the walls were computed. In the region close to the lens a strong stress concentration was found, which is essentially related to the larger Velocity reached by the fluid in that region due to the concavity of the wall.

Acknowledgments

This work has been developed within the framework of the project FIRB2001 (RBAU01Z44F005) co-funded by the MIUR. The authors gratefully acknowledge many useful discussions with Dr Andrea Scupola and Dr Sergio Petroni from the Gemelli Hospital of Rome, who provided clinical motivations for the present research.

References

Becker W 1989 *The Neurobiology of Saccadic Eye Movements* ed R H Wurtz and M E Goldberg (Amsterdam: Elsevier)

Canning C R, Dewynne J N, Fitt A D and Greaney M J 2002 Fluid flow in the anterior chamber of a human eye *J. Math. Appl. Med. Biol.* **19** 31–60

Cicekli U 2003 Computational model for heat transfer in the human eye using the finite element method *PhD Thesis* Louisiana State University

David T, Smye S, Dabbs T and James T 1998 A model for the fluid motion of vitreous humour of the human eye during saccadic movement *Phys. Med. Biol.* **43** 1385–99

Flyckt V M M, Raaymakers B W and Lagendijk J J W 2006 Modelling the impact of blood flow on the temperature distribution in the human eye and in the orbit: fixed heat transfer coefficients versus the Pennes bioheat model versus discrete blood vessels *Phys. Med. Biol.* **51** 5007–21

Graftieaux L, Michard M and Grosjan N 2001 Combining PIV, POD and vortex identification algorithms for the study of unsteady turbulent swirling flows *Meas. Sci. Technol.* **12** 1422–9

Lee B, Litt M and Buchsbaum G 1992 Rheology of the vitreous body: part I. Viscoelasticity of human vitreous *Biorheology* **29** 521–33

Loudon C and Tordesillas A 1998 The use of the dimensionless Womersley number to characterize the unsteady nature of internal flow *J. Theor. Biol.* **191** 63–78

Lund-Andersen H 2003 *Adler's Physiology of the Eye (Vitreous)* 10th edn, ed PL Kaufman and A Alm (Mosby) **See endnote 1**

Ottino J M 1989 *The Kinematics of Mixing: Stretching, Chaos, and Transport (Cambridge Texts in Applied Mathematics)* (Cambridge: Cambridge University Press)

Repetto R 2006 An analytical model of the dynamics of the liquefied vitreous induced by saccadic eye movements *Meccanica* **41** 101–17

Repetto R, Stocchino A and Cafferata C 2005 Experimental investigation of vitreous humour motion within a human eye model *Phys. Med. Biol.* **50** 4729–43

Scott J A 1988 A finite element model of the heat transport in the human eye *Phys. Med. Biol.* **33** 227–41

Endnotes

(1) Author: Please provide the place of the publisher in reference ‘Lund-Andersen 2003’
